Variations of Arctic winter ozone from the LIMS Level 3 dataset

Ellis Remsberg[1], Murali Natarajan[1], and Ernest Hilsenrath[2]

[1]Science Directorate, NASA Langley Research Center, 21 Langley Blvd, Mail Stop 401B, Hampton, VA 23681, USA

[2]Fellow at Joint Center for Earth System Technology, University of Maryland at Baltimore County, 1000 Hilltop Circle, Baltimore, MD 21250, USA

Correspondence to: Ellis Remsberg (ellis.e.remsberg@nasa.gov)

(for submission to Atmospheric Measurement Techniques Journal)

~~January~~February, 2022

Abstract

The Nimbus 7 limb infrared monitor of the stratosphere (LIMS) instrument operated from October 25, 1978, through May 28, 1979. Its Version 6 (V6) profiles and their Level 3 or zonal Fourier coefficient products have been characterized and archived in 2008 and in 2011, respectively. This paper focuses on the value and use of daily ozone maps from Level 3, based on a gridding of its zonal coefficients. We present maps of V6 ozone on pressure surfaces and compare them with several rocket-borne chemiluminescent ozone measurements that extend into the lower mesosphere. We illustrate how the synoptic maps of V6 ozone and temperature are an important aid in interpreting satellite limb-infrared emission versus local measurements, especially when they occur during dynamically active periods of northern hemisphere winter. A map sequence spanning the minor stratospheric warmings of late January and early February characterizes the evolution of a low ozone pocket (LOP) at that time. We also present time series of the wintertime tertiary ozone maximum and its associated zonally varying temperatures in the upper mesosphere. These examples provide guidance to researchers for further exploratory analyses of the daily maps of middle atmosphere ozone from LIMS.

1   Introduction and objectives

The historic Nimbus 7 Limb Infrared Monitor of the Stratosphere (LIMS) experiment provided data on middle atmosphere ozone from October 25, 1978, through May 28, 1979, for scientific analysis and for comparisons with atmospheric models (Gille and Russell, 1984). Ozone is an excellent tracer of stratospheric transport in the high latitude stratosphere. As an early example, Leovy et al. (1985) showed how daily maps of the LIMS ozone fields correlate well with geopotential height (GPH) fields on the 10-hPa pressure surface. They also reported on the rapidly changing effects of wave activity on ozone, which led to a better understanding of stratospheric transport processes within models. Hitchman et al. (1989) also analyzed the temperature fields from LIMS and reported on Arctic observations of an elevated stratopause in late autumn to early winter that they associated with momentum forcings from gravity waves.

Current research focuses on the 3-dimensional character of ozone in the upper stratosphere and mesosphere, based on more recent satellite datasets. Several studies consider how temperature and ozone vary in association with sudden stratospheric warming (SSW) events (Smith et al., 2009; de la Camara et al., 2018; Kim et al., 2020; Shams et al., 2021). Manney et al. (1995) and Harvey et al. (2008) describe the development of low ozone pockets (LOPs) in the region of the Aleutian anticyclone during winter. Siskind et al. (2005; 2021) explain the occurrence of a mesospheric cooling associated with SSWs and the role of gravity waves for modeling ozone in the upper mesosphere, respectively. Chandran et al. (2013) provide a climatology of the Arctic elevated stratopause, and Sofieva et al. (2021) analyze for regional trends in stratospheric ozone. Smith et al. (2011; 2018) report on monthly changes of the tertiary ozone maximum at high latitudes of the upper mesosphere during winter.

The LIMS (Level 2) profiles were retrieved with an improved Version 6 (V6) algorithm. They were archived in 2008 and include ozone, temperature, and GPH that extend from 316 hPa to ~0.01 hPa. Co-located V6 profiles of water vapor (H_2O), nitric acid vapor (HNO_3), and nitrogen dioxide (NO_2) extend through the stratosphere. Lieberman et al. (2004) analyzed the V6 temperature profiles and found evidence for non-migrating tides in the mesosphere, due to the interaction of the diurnal tide and planetary zonal-wave 1, especially in late January 1979. Holt et al. (2010) analyzed the descent of V6 NO_2 from the lower mesosphere to within the polar stratospheric vortex, where it interacts with ozone. Remsberg et al. (2013) assimilated V6 ozone profiles in a reanalysis model and gained improved estimates of column ozone, especially in Arctic winter. Such reanalysis studies assimilate temperature and ozone profiles within a model framework. However, the models only approximate the effects of small-scale variations, so it is also useful to consider observed variations of the LIMS parameters without resort to a model. Keep in mind that smaller-scale atmospheric variations also contribute to the analyzed intermediate and large-scale fields from V6. This paper further explores several instances of those larger-scale variations of Arctic ozone, temperature, and GPH.

The SPARC Data Initiative (SPARC-DI) includes monthly zonal averages of V6 ozone up to the 0.1-hPa level (see Tegtmeier et al., 2013; SPARC, 2017; and Remsberg et al., 2021). In Section

78 2 we show January zonal averages of V6 ozone and temperature profiles that extend even higher

79 or to near the mesopause. The V6 Level 3 (map) product provides a 3-dimensional context for

80 those zonal mean data. Daily V6 maps are also an aid in interpretating individual V6 profiles

81 versus correlative data, especially during dynamically disturbed periods. Specifically, in Section

82 3 we compare several nighttime V6 ozone profiles with those obtained with a rocket-borne

83 chemiluminescent technique (Hilsenrath et al., 1980). Those profile comparisons are for

84 December 15 and for January 27 and 28, when the temperature and ozone fields were affected by

85 planetary wave forcings. There is a corresponding cooling and variations of ozone in the winter

86 lower mesosphere associated with the warming in the upper stratosphere. Section 4 presents

87 variations of ozone and GPH at northern extratropical latitudes during the minor SSW events of

88 late January and early February 1979, as a complement to the more comprehensive findings of

89 Harvey et al. (2008) on the occurrence of LOPs within anticyclones determined from satellite

90 solar occultation data. Section 5 considers the variability of the tertiary ozone maximum in the

91 upper mesosphere during that same period, as an adjunct to monthly zonal average values

92 reported by Smith et al. (2018). Section 6 notes that the maps of V6 ozone contain more details

93 about ~~the~~ gradients ~~of atmospheric~~in temperature and ozone ~~during disturbed periods, but~~

94 ~~also~~and cautions users about occasional, pseudo-ozone features in the tropical lowermost

95 stratosphere. Section 7 concludes that the V6 Level 3 product ~~represents~~is an important resource

96 for studies of the effects of transport and chemistry on Arctic ozone.

97

98 **2   Characteristics of V6 Level 3 data**

99 *2.1 LIMS measurements and analyses*

100 Nimbus 7 was in a near-polar orbit, and LIMS made measurements at ~1 pm local time along its

101 ascending (A or south-to-north) orbital segments and at ~11 pm on its descending (D or north-to-

102 south) segments. A-D time differences are of the order of 10 hours at most latitudes because

103 LIMS viewed the atmosphere 146.5° clockwise of the spacecraft velocity vector, as seen from

104 above. The A-D differences narrow from 10 to about 6 hours from 60°N to 80°N, due to the

105 orbital geometry of Nimbus 7. The V6 processing algorithm accounts for low-frequency

106 spacecraft motions that affect the LIMS view of the horizon. As a result, its measured radiance

107 profiles are well registered in pressure-altitude (Remsberg et al., 2004). Retrieved V6 ozone,

108   temperature, and GPH profiles extend from 316 hPa to ~0.01 hPa and have a vertical point

109   spacing of ~0.88 km with an altitude resolution of ~3.7 km. Retrieved profile pairs are spaced

110   every 144 km along the orbital track or at every 1.3°, but closer together at the high, turn-around

111   latitudes of the orbital viewing geometry (Remsberg et al., 1990). LIMS made measurements

112   with a duty cycle of about 11 days on and 1 day off over its planned observing lifetime. The

113   LIMS algorithms (Remsberg et al., 2007) do not account for non-local thermodynamic

114   equilibrium (NLTE) effects in ozone (Solomon et al., 1986; Mlynczak and Drayson, 1990) and

115   in CO_2 (Edwards et al., 1996; Manuilova et al., 1998), so there are positive biases in the retrieved

116   V6 ozone throughout the mesosphere during daylight. However, the V6 nighttime ozone is more

117   nearly free of NLTE effects below about the 0.05-hPa level, except at times of SSWs (see e.g.,

118   Funke et al., 2012).

119

120   A sequential-estimation (SE) algorithm was used to generate daily, zonal Fourier coefficients

121   (zonal mean and up to six cosine and sine values or 6-zonal wavenumbers) for Level 3 at every

122   2° of latitude and at up to 28 vertical levels (Remsberg and Lingenfelser, 2010). The V6 SE

123   algorithm uses better estimates of data uncertainty and its zonal wave coefficients have a

124   memory of ~2.5 days, or about half that of the SE algorithm used by Remsberg et al. (1990).

125   The SE analysis is insensitive to the very few large, unscreened ozone profiles values found in

126   the lower stratosphere, as noted in Remsberg et al. (2013, their Fig. 1a). The SE algorithm

127   combines the coefficients from both the separate A and D orbital segments and effectively

128   interpolates the profile data in time to provide a continuous, 216-day set of daily zonal

129   coefficients versus pressure-altitude at 1200Z for each of the retrieved LIMS parameters.

130

131   *2.2 Monthly average V6 data*

132   One can generate monthly average distributions from the daily Level 3 files of temperature,

133   GPH, and species (ozone, H_2O, HNO_3, and NO_2); zonal averages for the V6 species were

134   supplied to SPARC-DI (SPARC, 2017; Hegglin et al., 2021). Tegtmeier et al. (2013) compared

135   the V6 monthly ozone distributions with ones from other satellite-based, limb sensors and

136   reported good agreement throughout the stratosphere. Although the species cross sections for

137   SPARC (2017) extend only up to the 0.1-hPa level (~64 km), V6 average ozone extends higher

138   or to about 0.015 hPa (~75 km). Figure 1 shows the latitude-pressure cross section for January

139   from just the descending (D) orbital profiles, which avoids the larger NLTE biases that affect

140   daytime ozone in the mesosphere. Stratospheric ozone mixing ratios in Fig. 1 have largest

141   values at about 10 hPa near the Equator (> 9.2 ppmv), and they decrease sharply above and

142   below that level. Maximum mixing ratios for the middle to high latitudes occur between 3 to 5

143   hPa, due to the larger zenith angles and longer paths of the ultraviolet light for production of

144   atmospheric ozone. There is a nighttime ozone minimum of ~1.2 ppmv across most latitudes of

145   the middle mesosphere. A tertiary ozone maximum is present in the upper mesosphere near the

146   winter day/night terminator zone in the LIMS measurements for January (at about 67°N), in

147   accordance with the interpretation of Marsh et al. (2001). The location (~0.02 hPa) and

148   magnitude (~3.5 ppmv) of the NH maximum are somewhat higher and larger than those reported

149   by Smith et al. (2018, their Fig. 4) from more recent satellite datasets. ~~On the other hand,~~

150   ~~while~~Although the V6 ozone poleward of ~~~50~~55°S is also from descending orbital profiles, it

151   corresponds to daylight conditions at the high southern latitudes in January. Thus, the decrease

152   of mesospheric V6 ozone at 0.1 hPa and poleward of ~~50~~55°S ~~in Fig. 1~~ indicates merely a change

153   from night to day values and agrees with findings of Lopez-Puertas et al. ~~(2018).~~(2018). On the

154   other hand, the rather large ozone values in the upper mesosphere at about 45°S are not found in

155   other data sets and are not expected from theory. We consider that ozone anomaly further in

156   Section 6.

157

158   Radiances from two 15-μm CO_2 channels are used for retrievals of V6 temperature versus

159   pressure or T(p), and they are free of NLTE effects below about the 0.05-hPa level (~70 km)

160   (Lopez-Puertas and Taylor, 2001). To first order, the V6 T(p) retrievals account for the effects

161   of horizontal temperature gradients in the stratosphere (Remsberg et al., 2004). Single profile

162   root-sum-squared (or RSS) errors for T(p) vary from 1 K at 10 hPa to ~2.5 K in the upper

163   mesosphere, but they do not include possible temperature gradient errors. RSS error from T(p) is

164   the primary source of bias error for ozone, growing to about 16% in the middle mesosphere

165   (Remsberg et al., 2021, Table 1). Random errors become large for single ozone profiles in the

166   upper mesosphere. As a complement to the V6 ozone of Fig. 1, we show the descending

167 (~nighttime) V6 T(p) distribution for January in Figure 2, which extends to near the 0.01-hPa

168 level. The large-scale features of the T(p) distribution compare well with climatological values

169 from the late 1970s (Fleming et al., 1990), having a maximum value of about 285 K at the SH

170 high latitude stratopause and minimum values of < 200 K at the tropical tropopause and near the

171 SH summer mesopause. There is also some elevation of the Arctic zonal-average stratopause.

172

173 Figure 3 shows the monthly-average, zonal (wave) standard deviations (SD) about daily zonal

174 means of the combined-mode (A+D) V6 ozone for January, where the SD values are derived

175 from the zonal-wave amplitudes of V6 Level 3. There are relatively small SD values at low

176 latitudes from 7 to 10 hPa; it is assumed that they are a result of smaller-amplitude Kelvin and

177 Rossby-gravity waves. Effects of more vigorous, planetary wave activity are most apparent at

178 high northern latitudes of the stratosphere during winter. Gravity waves also contribute to SD in

179 the uppermost mesosphere (Siskind et al., 2021). Ozone shows little zonal variation in the SH

180 upper stratosphere of Fig. 3, due to constraints on the upward propagation of planetary waves

181 through the summer zonal easterlies (Andrews et al., 1987). SD values near the tropical

182 tropopause are due mostly to residual effects of emissions from thin cirrus and represent spurious

183 ozone variations (see Section 6).

184

3.   V6 comparisons with rocket-borne chemiluminescent ozone measurements

186 In this section we consider V6 comparisons with three nighttime, rocket-borne chemiluminescent

187 ozone soundings of Hilsenrath (1980)—one at White Sands, NM, (32.4°N, 253.5°E) on

188 December 15, 1978, and two more at Poker Flat, AK, (65.1°N, 212.5°E) on the successive days

189 of January 27 and 28, 1979. The estimated total, rocket ozone error is 14% (precision plus

190 accuracy), according to Hilsenrath and Kirschner (1980).

191

192 Ozone comparisons for December 15 are in Figure 4 (top); we plot every other V6 profile and

193 those four profiles have spacings of 2.6° in latitude. The short-dashed V6 profile is at 29.2°, and

194 the long-dashed profile is at 37.2°. The solid curve is the V6 profile at 31.8° (at 0611Z) or

195 closest to the rocket sounding from White Sands (at 0541Z). Horizontal bars on the profiles are

196 estimates of ozone error; they overlap between V6 and rocket, except in the upper stratosphere.

197 LIMS ozone is larger than rocket ozone in through the upper stratosphere. The corresponding

198 V6 ozone map at 4.6 hPa in Fig. 4 (bottom) reveals an ozone maximum just south of White

199 Sands (WS—blue dot), along the descending orbital segment of the satellite at (6°N, 265°E—

200 white dot) or viewing in the NNW direction toward White Sands. Note that while zonal

201 variations in the map are from a gridding of the Level 3 coefficients (2° latitude and 5.625°

202 longitude), there is no smoothing of the gridded field in the meridional direction; there is good

203 continuity across latitudes, nonetheless. The rocket profile is a local measurement and has a

204 vertical resolution that ranges from 1.5 km at 60 km to 0.1 km at 20 km; the nearby V6 profiles

205 have a lower vertical resolution of ~3.7 km and are an average over the finite horizontal length

206 (~300 km or ~3° latitude) of the LIMS tangent layer. There is an ozone maximum along the

207 LIMS view path just to the south of White Sands, which may account for the profile differences.

208 We also note that the ozone field of two days earlier has the region of sharp gradients positioned

209 over White Sands with ozone at only 8 ppmv. Thus, an ozone field that varies in both space and

210 time can lead to additional uncertainties for comparisons of the localized rocket and limb-

211 viewing satellite profiles in Fig. 4.

212

213 Because V6 ozone is obtained from retrievals of the measured V6 ozone radiance profiles, the

214 LIMS retrieved temperature profile must be representative of the atmospheric state for the

215 forward model of ozone radiance. Figure 5 (top) shows the corresponding temperature

216 comparisons between V6 and a separate rocket Datasonde instrument. Agreement between them

217 is very good throughout the upper stratosphere, indicating that the temperature variations are

218 well determined along the LIMS view path for the forward radiance calculations of V6 ozone

219 and that the retrieved V6 ozone should be nearly unaffected by temperature bias error. The map

220 of V6 temperature (Fig. 5—bottom) shows zonal variations on December 15, although their

221 meridional gradients are relatively weak above White Sands. Conversely, the ozone profiles

222 agree well near 0.68 hPa in Fig. 4, where there are apparent biases between the T(p) profiles.

223 There are significant horizontal gradients near White Sands in the maps of T(p) at 0.68 hPa, but

224 not in ozone (not shown). In fact, the V6 ozone field at that level has a nearly constant value,

225 and ozone is less sensitive (by half) to changes in T(p) at 0.68 hPa than at 4.6 hPa (Remsberg et

226 al., 2007). Co-location is more important for the V6 versus rocket comparisons of T(p) than of

227 ozone in the lower mesosphere.

228

229 The two comparisons above Poker Flat, AK, occurred at the time of a stratospheric, zonal wave-

230 1 warming event. Leovy et al. (1985) provide a detailed discussion of the advective changes for

231 ozone in the middle stratosphere during January 1979. Figure 6 (top) shows three V6 ozone

232 profiles from along an ascending orbital segment on January 27. The LIMS instrument was

233 viewing from its satellite location (80.7°N, 113°E) at 2204Z, and the rocket ozone launch was

234 two hours earlier or at 2005Z at a solar zenith angle of 84° or near the terminator; there is good

235 agreement of the structure between them, even in the mesosphere. A second rocket launch

236 followed at 0833Z of January 28 (Hilsenrath, 1980). Since the separate V6/rocket ozone and

237 T(p) comparisons are similar for the two days, Fig. 6 contains results for January 27 only. The

238 rocket sounding recorded two ozone maxima, one near 15 hPa and another at about 0.6 hPa. The

239 ozone maximum at about 15 hPa is primarily due to advection of ozone of higher mixing ratios

240 from lower latitudes just prior to the warming event. The local maximum at 0.6 hPa was

241 unexpected, based on findings from a larger set of rocket ozone soundings. There is a relative

242 minimum for both V6 and rocket ozone through the upper stratosphere, although V6 ozone is

243 larger. The map of V6 ozone at 4.6 hPa in Fig. 6 (bottom) indicates that the rocket measurement

244 occurs at the center of the minimum, whereas the V6 profiles are averages across it. The ozone

245 profiles in Fig. 6 (top) indicate the relative minimum in a low-ozone pocket (LOP) that extends

246 from about 7 hPa to 2 hPa.

247

248 Figure 7 (top) shows the V6 temperature profile comparisons; T(p) from the Datasonde has more

249 vertical structure, as expected from a localized measurement. V6 T(p) values reach a maximum

250 of order 250 K at about 3 to 4 hPa. They agree reasonably with the Datasonde values, given that

251 there is significant horizontal structure in the temperature field surrounding Poker Flat. The

252 apparent V6 minus Datasonde bias of order 5 K at 3 hPa ought to lead to a V6 minus rocket

253 ozone bias of -40%, according to error estimates for retrieved V6 ozone. However, Fig. 7

254 (bottom left) indicates that LIMS was viewing Poker Flat across an area of higher temperatures,

255 such that it is likely that there is a spatial mismatch for V6 and Datasonde T(p) values. The
256 much smaller and positive ozone differences in Fig. 6 support that likelihood. There may also be
257 co-location differences between the rocket temperature and ozone soundings in this instance.

258

259 Figure 7 also shows a map of NH GPH at 4.6 hPa on January 27 for comparison with the ozone
260 map in Fig. 6. Lowest ozone values are in the polar vortex, where the GPH field is asymmetric
261 about the Pole. A second, low value of ozone is associated with the anticyclone over the
262 Alaskan sector. One can determine horizontal winds from gradients of GPH on the 4.6-hPa
263 surface and thereby estimate the transport of ozone to first order. Qualitatively, the direction and
264 strength of the large-scale transport follows from the character of the cyclonic and anticyclonic
265 features on the GPH map. The large-scale cyclonic circulation about the vortex transports air
266 from middle latitudes to across the Pole on January 27. The vortex region has low ozone and is
267 relatively cold, whereas stratospheric temperatures over Alaska show a maximum (the SSW),
268 and the rocket profile above Poker Flat, AK, was near the center of the anticyclone and in the
269 region of relatively low ozone (or LOP).

270

271 Ozone is an approximate tracer of transport processes and reveals dramatic changes with altitude
272 associated with this SSW event, even through the winter lower mesosphere. As an example,
273 Figure S1 (in Supplemental Materials) shows a concurrent cooling at 0.46 hPa above the Alaskan
274 anticyclone on January 27, where the co-located ozone field exhibits a local maximum. There is
275 also a major temperature increase above the polar stratospheric vortex over northern Europe at
276 0.46 hPa, or where ozone values remain low. In summary, Figs. 4 through 7 and S1 indicate the
277 utility of daily maps from LIMS for analyses of the ozone fields during dynamically disturbed
278 conditions.

279

280 **4. Variation of a low ozone pocket (LOP) from LIMS Level 3**

281 The polar vortex on January 27 was located over northern Europe and Asia; it was centered off
282 the Pole because of effects of large-scale, planetary waves in the development of the SSW

283 (Andrews et al., 1987, Chapter 6). In this section, we show sequences of polar plots of both

284 stratospheric GPH and ozone for February 1979. Manney et al. (1995) and Harvey et al. (2004,

285 2008) provide comprehensive analyses about the occurrence of polar anticyclones and their

286 associated LOPs from studies of GPH and ozone fields from several different satellites. They

287 determined the extent and character of the polar vortex based on meteorological data from the

288 UK Met Office or as obtained from relatively low vertical resolution radiance profiles from

289 operational, nadir temperature sounders. The V6 GPH profiles are derived from and have the

290 same vertical resolution as the T(p) profiles. Manney et al. (1995) showed that water vapor is a

291 useful tracer of the meridional transport of air, and the V6 H_2O fields at 6.8 and 10 hPa indicate

292 that low latitude air was transported to the region of the LOP in late January. But the V6 H_2O

293 fields are noisy at 4.6 hPa (not shown). Even so, the V6 Level 3 ozone, T(p), and GPH data

294 offer useful details about the occurrence of LOPs in the upper stratosphere.

295

296 Harvey et al. (2004) reported that LOPs occur nominally at about the 5-hPa level. Accordingly,

297 the three panels of Figure 8 show three daily NH maps of V6 GPH from February 3 to February

298 17 at 4.6 hPa; each successive map is spaced one week from the previous one. This sequence

299 shows that both the vortex and anticyclone weaken during the three weeks following January 27

300 at this level. The vortex re-centers on the Pole by February 17, and the anticyclone is nearly

301 absent at 4.6 hPa following the two minor warming events. The map sequence of GPH indicates

302 that there were significant changes in the horizontal transport of ozone in late January/early

303 February. The corresponding three panels of ozone in Figure 9 show the further evolution of

304 ozone, following that of January 27 (in Fig. 6). Even though the anticyclone had weakened

305 during the first week, there was a deepening of the LOP from January 27 to February 3 and a

306 filling of it thereafter.

307

308 Was there some chemical loss of ozone from January 27 to February 3 in the region of the LOP?

309 Morris et al. (1998) and Nair et al. (1998) conducted model calculations to show how that could

310 happen. Ozone reactions are affected by changes with latitude of solar insolation, temperature,

311 and loss via NO_x. Nair et al. (1998) reported on the effect of a decrease in the production of

312 ozone for the development of LOPs, as air parcels in the middle stratosphere move from low to

313 high latitudes or to higher solar zenith angles in winter. Remsberg et al. (2018) analyzed air

314 parcel trajectories that included chemistry, and they showed that there was some loss of ozone in

315 the middle stratosphere, due to reactions with NO_x. However, Holt et al. (2012) analyzed V6

316 NO_2 in the winter polar vortex, and they did not find enhanced values at 4.6 hPa due to energetic

317 particle precipitation (EPP) by late January.

318

319 Figure 10 (left) is a map of the V6 descending orbital (nighttime) NO_2 for January 27 at 4.6 hPa.

320 Based on the corresponding map of GPH in Fig. 7, one can trace the horizontal advection of high

321 NO_2 toward higher latitudes and toward the polar vortex as well as the advection of low NO_2 out

322 of the vortex and about the anticyclone. Fig. ~~10 (right) is a map of HNO₃ at 4.6 hPa. It has a~~

323 ~~weak, relative maximum above the anticyclone that appears as a residual from the advection of~~

324 ~~much higher vortex values from several days before. A closer inspection in time reveals that the~~

325 ~~NO₂ values in the LOP were a bit lower by January 31, when ozone had already declined to near~~

326 ~~its February 3 value. Thus, while an excess of HNO₃ in the region of the LOP is consistent with~~

327 ~~a conversion of NO₂ to HNO₃ above the isolated anticyclone, there is no clear evidence from the~~

328 ~~V6 map products that such chemistry led to significant changes in the ozone. One must conduct~~

329 ~~trajectory studies that include chemistry and that rely on the V6 species profiles as input for~~

330 ~~better, quantitative estimates. Unfortunately, the profiles of V6 NO₂ and HNO₃ become noisy in~~

331 ~~the upper stratosphere. At a minimum though, one can follow the evolution of the LOP using the~~

332 ~~daily maps of V6 ozone and GPH.~~ 10 (right) is a map of HNO_3 at 4.6 hPa, and it shows a weak,

333 relative maximum above the anticyclone.

334

335 The formation of the LOP at 5hPa near Poker Flat region in January is studied with the help of

336 photochemical calculations along a trajectory. A full description of the trajectory and

337 photochemical models is given in Remsberg et al (2018). For this study, we generated backward

338 trajectory starting at 5 hPa and 212° E and 64°N. The starting time of the back trajectory is 0900

339 Z on January 28,1979. This is close to local time of LIMS descending mode observation of

340 around 11:00 pm on January 27. Figure 11 shows the back trajectory with the day numbers

341 illustrating the progress of the air parcel. Between January 22 and 28, the air parcel remains

342 confined within a small region at high latitude. Results of a time dependent photochemical

calculation conducted along this trajectory in the forward direction are shown in Figure 12 as a function of time. The model initialization uses the mixing ratios of O_3, NO_2, and HNO_3 from LIMS descending mode observations. Figure 12 shows that the parcel was at 3 hPa on January 15 and descended steadily to 5 hPa by late January. The decrease in ozone during the last 8 days is mainly caused by the daytime odd oxygen loss due to the catalytic cycle involving NO_x. Production of odd oxygen is minimized since the air parcel is confined to high latitudes. Large diurnal variations in NO_2 and a small increase in HNO_3 are as expected for this pressure level. The LOP formation is a result of the interplay between transport and photochemistry in the high latitude upper stratosphere in the winter.

5. Variations of the tertiary ozone maximum

Smith et al. (2018) describe the changing monthly, zonally averaged character of the wintertime tertiary ozone maximum of the polar upper mesosphere. They point out that the low latitude edge of the tertiary ozone maximum is where HO_x radicals and the chemical loss of ozone due to reactions with them are reduced. V6 ozone radiance profiles have low signal-to-noise in the upper mesosphere; the precision estimate is 0.32 ppmv for retrieved ozone profiles. We show a map in Figure 1113 of the combined V6 ozone for December 15 at 0.022 hPa (~72 km), where its distribution in the subpolar region is based on fewer than 13 zonal coefficients because some profiles do not extend to that pressure altitude. The corresponding map of temperature is also in Fig. 1113, and one can see that there is significant non-zonal structure in its field at the latitudes where ozone is enhanced. While both V6 ozone and temperature are not highly accurate due to NLTE effects in the upper mesosphere, their maps reveal significant relative spatial structures indicating advective transport and its likely effects on ozone.

Figures S2 and S3 in the Supplemental Materials show additional panels at 0.022 hPa of ozone and temperature, respectively, for January 13, February 10, and March 1. Elevated values of ozone occur at higher latitudes on February 10 and March 1 than on December 15 and January 13, which is consistent with the more northward position of the terminator away from winter solstice and the consequent effects for the chemical loss of ozone. The temperature fields are

372 also perturbed on January 13 and February 10, but they are more nearly zonal by March 1.

373 However, there are meridional gradients of temperature on all three days in the region of the

374 tertiary ozone maximum. On January 13 there is also a well-defined mesospheric vortex in GPH

375 (not shown), and the highest values of ozone correlate reasonably with it. The vortex is most

376 disturbed and tertiary ozone maximum has largest values on February 10, perhaps in response to

377 the upward propagation of wave activity following the minor SSW of late January.

378

379 Figure 1214 shows time series of peak zonal mean ozone at 0.022 hPa and its latitude location

380 for each week from November through mid-March. The separate time series are for peak ozone

381 (bottom two series) and their latitude locations (top two). Dashed red curves represent zonal

382 mean results for combined (A+D) ozone; solid black curves are results for nighttime (D) only.

383 Blue horizontal lines represent the approximate latitude position of the terminator. Peak

384 nighttime ozone values are based on just the 'zonal mean' and the cosine and sine coefficients

385 for waves 1 and 2 because not all profiles reach to the 0.022-hPa level. Peak ozone occurs at

386 lower latitudes (~65°N) in December, increasing to ~75°N in early November and early February

387 and to near 80°N by early March. The latitude time series of peak ozone values is reasonably

388 coincident with the changing location of the terminator. Peak combined (A+D) ozone increases

389 slowly from a minimum of 2.2 ppmv in November to 3.6 ppmv in late February and March.

390 Descending (or nighttime only) ozone varies from 3.3 ppmv in November, to ~4.5 ppmv in

391 January, to a maximum of 6.3 ppmv in mid-February, and then declining to 3.5 ppmv by mid-

392 March, although the time series shows rather large variations. Those maximum V6 values are

393 larger than reported by Lopez-Puertas et al. (2018, their Fig. 15), perhaps due to biases from V6

394 T(p) and/or ozone at 0.022 hPa.

395

396 The increasingincrease of V6 ozone in Fig. 12 during winter in Fig. 14 disagrees with that of

397 Smith et al. (2018), who found decreasing ozone inby February. They reported that, in most

398 years, there is a slow descent of relatively dry air into the vortex region in the upper mesosphere

399 during late autumn and early winter in the upper mesosphere, and that the reduction in water

400 vapor implies that there are fewer HO_x radicals for the destruction of ozone near the terminator

401 zone, leading to accumulations of ozone. However, there were two minor warmings and

402 associated lower mesospheric cooling events during late January and early February 1979

403 (Hitchman et al., 1989). The enhanced V6 ozone of February 1979 follows those SSW events~~.~~

404 ~~It may be that~~~~ .~~, and there ~~were~~are wave-driven disturbances and ~~a~~dissipation of their energy in

405 the upper mesosphere at ~~higher latitudes at~~ that time (e.g., Siskind et al. 2005~~).~~; Smith et al.,

406 2009). One ~~should be able to~~can gain more ~~information~~details about the evolution of the tertiary

407 ozone maximum in the winter of 1978-79 from the daily maps of V6 ozone, T(p), and GPH (as

408 in Figs. S2 and S3).

409

410 **6. Other aspects of V6 Level 3 ozone**

411 The combined (A+D) Level 3 coefficients are the basis for a gridding of daily synoptic maps at

412 1200Z of ozone and related parameters. The Level 3 product also contains coefficients from its

413 separate A and D profiles; their 'zonal mean' values correspond to the local time-of-day of their

414 respective measurements. Remsberg et al. (2007) noted that maps from V6 reveal more details

415 about the variations of ozone. In Figure S4 of the Supplemental ~~Material~~Materials we compare a

416 map of V6 ozone at 10 hPa on 27 January with a similar map for V5 of Leovy et al. (1985). The

417 ozone gradients are more pronounced with V6 than with V5 at both the subtropical and vortex

418 edges of the ozone field.   The V6 maps make use of all profiles along the orbit, and the SE

419 mapping algorithm was applied to them every 2° of latitude. However, the tighter gradients were

420 also achieved with the V6 algorithm because it has a relaxation time (or memory) that is half that

421 of V5. This means that the V6 maps are more representative of the rapidly changing

422 atmospheric ozone fields on that day. Similar version differences are evident throughout winter,

423 when the so-called 'stratospheric surf zone' develops and expands (Leovy et al., 1985).

424

425 Significant exchanges of air and ozone occur from the extratropical stratosphere to the

426 troposphere in winter and spring (Gettelman et al., 2011). There are large zonal variations about

427 the daily zonal means of ozone in the Arctic region of the lower stratosphere in Fig. 3. There are

428 similar variations in GPH (and derived winds) and in zonal wave activity that lead to ozone

429 transport. Zonal variations are resolved in the daily ozone maps down to the 146-hPa level.

430 Notably, Shepherd et al. (2014) integrated the V6 monthly zonal mean ozone above the

431 tropopause and subtracted it from observed total ozone, as part of their assessment of long-term

432 trends of tropospheric ozone from models. Their determination of extratropical tropospheric

433 ozone based on LIMS agrees with that obtained from other ozone datasets.

434

435 There is also a relative excess of SD ozone values in Fig. 3 centered at 68 hPa at tropical

436 latitudes, and similar anomalies occur in other LIMS months (not shown). As an example,

437 Figure 1315 shows a map of V6 ozone at 68 hPa (~18 km) on December 15, to give more insight

438 about the source of the tropical variations. Ozone mixing ratio values in Fig. 1315 are of order 2

439 to 3 ppmv at high latitudes, becoming much smaller in the subtropics. However, there is also an

440 unexpected, high value of 2 to 3 ppmv at about 15°N, 150°E. Limb measurements in the ozone

441 channel include radiance effects from cirrus particles that can occur along the tangent view path,

442 although the retrieved ozone mixing ratio profiles were screened of those effects to first order

443 (Remsberg et al., 2007). Even so, we note that ozone is easily affected by any excess radiance

444 because of highly non-linear effects for retrievals of ozone in the lower stratosphere. It is very

445 likely that the anomalous ozone at 68 hPa is a result of residual effects from subvisible cirrus,

446 which is nearly ubiquitous over the western tropical Pacific region (see SPARC, 2006, Fig. 1.8).

447 While individual V6 ozone profiles may include such spurious features in the tropics, the Level 3

448 ozone product at 68 hPa is affected mainly when there is an organized convection and outflow of

449 air that persists for several days. The adjacent map of ozone at 46 hPa appears unperturbed in

450 that region (not shown), and tropical ozone at 100 hPa approaches zero. There are much smaller

451 anomalies in maps of nitric acid, as its mixing ratio retrieval is very nearly linear. Anomalies are

452 also not so apparent in maps of V6 H_2O at 68 hPa because the cloud screening algorithm for H_2O

453 accounts for the larger vertical field-of-view and extent in altitude for measurements in the water

454 vapor channel of LIMS. To summarizeThus, one must be mindful that the Level 3 product may

455 indicate excess, but spurious ozone at 68 hPa in the tropics.

456

457 Finally, in our earlier description of descending orbital ozone in Fig. 1, we noted that there are

458 anomalously high values near 45°S in the upper mesosphere. Fig. S5 of the Supplemental

459 Materials shows distributions of temperature and ozone from descending orbital measurements at

460 0.032 hPa on January 15. Zonal wave activity is very weak in both. The descending orbital

views of the tangent layer at 45°S are located just in front of the region of large temperature gradients at 40°S. Although we showed in Section 3 that taking account of temperature gradients is important for accurate retrievals of ozone, such gradients were not employed for calculations in the mesosphere of tangent layer radiance in the V6 algorithms. If such temperature biases persist through the upper mesosphere, they will also affect the registration of the observed ozone radiance versus pressure at those altitudes. Therefore, we judge that it is very likely that the enhanced ozone mixing ratios near 45°S in Fig. 1 are an artifact because the associated, retrieved tangent path temperatures are not weighted properly, are too cold, and do not account for enough of the observed ozone radiance. Ozone mixing ratio anomalies are not apparent along the ascending orbital segment because their LIMS views are in a near-zonal direction.

7. Conclusions

This report provides guidance to researchers for their use of the LIMS V6 Level 3 product and for their generation of daily gridded distributions of its temperature, ozone, and GPH on pressure surfaces. H_2O, NO_2, and HNO_3 are also available for the stratosphere from the Level 3 product. The V6 dataset represents an early baseline for considering possible changes in the middle atmosphere from 1979 to today and into the future. LIMS made measurements at a time when stratospheric effects from volcanoes were minimal and when catalytic effects of chlorine on ozone were relatively small. Accordingly, Stolarski et al. (2012) found small, but significant changes in the distribution of upper stratospheric ozone for recent decades compared with 1978-1979. The LIMS measurements were taken near solar maximum and when atmospheric concentrations of the greenhouse gases (GHG), CO_2, CH_4, and CFCs, were smaller than today. Middle atmosphere T(p) distributions were warmer in 1978-1979.

The LIMS measurements in the winter Arctic region occurred when there was a lot of wave activity for the transport and mixing of ozone. As a result, ozone varied dramatically in winter, particularly during times of stratospheric warming events. There was a so-called Canadian warming in early December 1978, two minor SSW events in late January and early February,

490   and a final warming in late February 1979. We showed V6 comparisons with temperature and

491   ozone profile data obtained using rocket borne Datasonde and chemiluminescent instruments,

492   and we pointed out how an examination of changes in their nearby fields is valuable for the

493   interpretation and validation of V6 profiles against those correlative measurements. The Level 3

494   dataset provides daily details on variations of ozone with latitude, longitude, and altitude, along

495   with related variations in temperature, geopotential height, NO_2, and HNO_3. We noted also that

496   there are instances of spurious, excess ozone from the Level 3 coefficients at 68 hPa in the

497   tropics but not in the extratropical stratosphere.

498

499   We displayed evidence of a low ozone pocket (LOP) and its chemical properties at 5 hPa above

500   the Aleutian anticyclone during the minor SSW of late January above the Aleutian anticyclone,

501   and we followed its evolution into mid-February. The V6 nighttime ozone is relatively accurate

502   through the mesosphere in Arctic winter. We provided time series of the wintertime, tertiary

503   ozone maximum of the upper mesosphere from V6 data. Its ozone reached maximum values in

504   February, perhaps as a response to enhanced wave activity in the mesosphere following several

505   SSW events. Together with V6 maps of T(p) and GPH, one may explore further the daily

506   evolution of that ozone maximum throughout the NH winter of 1978-1979.

507

508   Data Availability

509   The LIMS V6 Level 3 product is at the NASA EARTHDATA site of EOSDIS and its website:

510   https://disc.gsfc.nasa.gov/datacollection/LIMSN7L3_006.html (Remsberg et al., 2011). The

511   SPARC-Data Initiative data are located at https://doi.org/10.5281/zenodo.4265393 (Hegglin et

512   al., 2021). We acknowledge the individual instrument teams and respective space agencies for

513   making their measurements available, and the Data Initiative of WCRP's (World Climate

514   Research Programme) SPARC (Stratospheric Processes and their Role in Climate) project for

515   organizing and coordinating the compilation of the chemical trace gas datasets used in this work.

516

517 *Author Contributions.* ER ~~wrote~~led the manuscript and prepared most of the figures with

518 contributions from his co-authors. MH conducted the trajectory study and generated its figures.

519 EH provided his rocketsonde data on ozone and temperature along with their error estimates.

520

521 *Competing interests*. The authors declare no competing interests for this study.

522

523 *Acknowledgements*. The authors appreciate John Gille and Jim Russell III and members of the

524 LIMS Science Team for their leadership in the development of the LIMS instrument and for their

525 processing of its historic data products. The authors are grateful to John Burton, Praful Bhatt,

526 Larry Gordley, B. Thomas Marshall, and R. E. Thompson for producing the V6 Level 2 dataset.

527 They acknowledge Gretchen Lingenfelser for her work in generating and archiving the V6 Level

528 3 coefficient dataset. They appreciate especially the constructive comments from the two

529 anonymous referees. They also thank V. Lynn Harvey for her comments on an early draft of the

530 manuscript. EER and MN carried out their work while serving as Distinguished Research

531 Associates of the Science Directorate at NASA Langley.

532

533

534

535
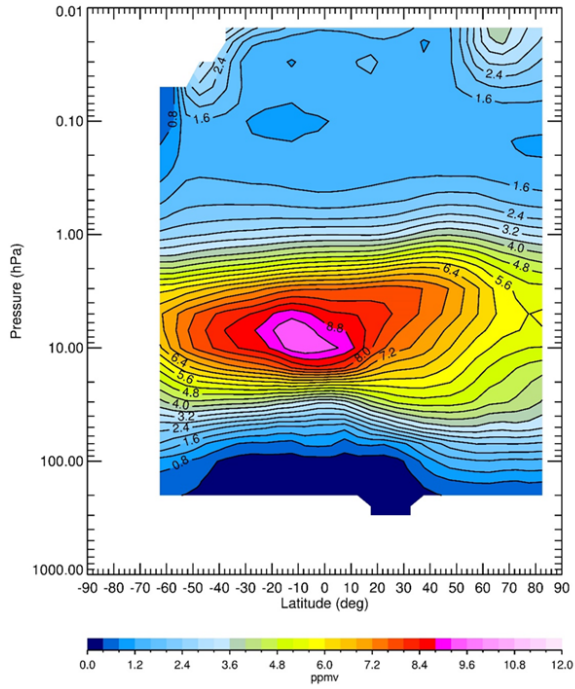
Figure 1—LIMS V6 Level 3 monthly zonal mean ozone for descending-mode only (or nighttime
equatorward of ~55°S) for January 1979. Contour interval (CI) is 0.4 ppmv.

538

539
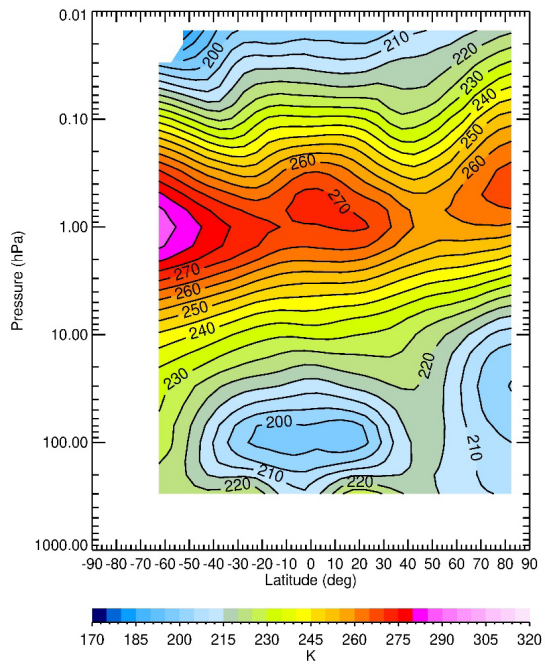
540

541   Figure 2—Zonal average, descending-mode, temperature for January 1979. CI is 5 K.

542

543

544

545
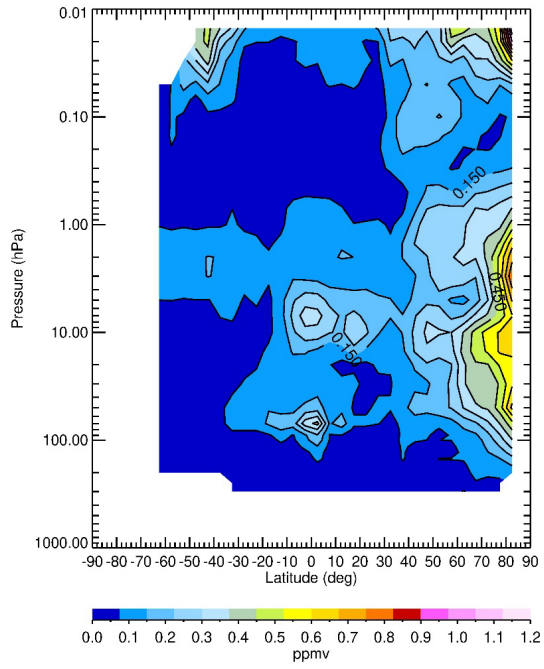
Figure 3—Zonal standard deviation about average (A+D) zonal mean ozone for January 1979.

CI is 0.075 ppmv.

548

549

550

551
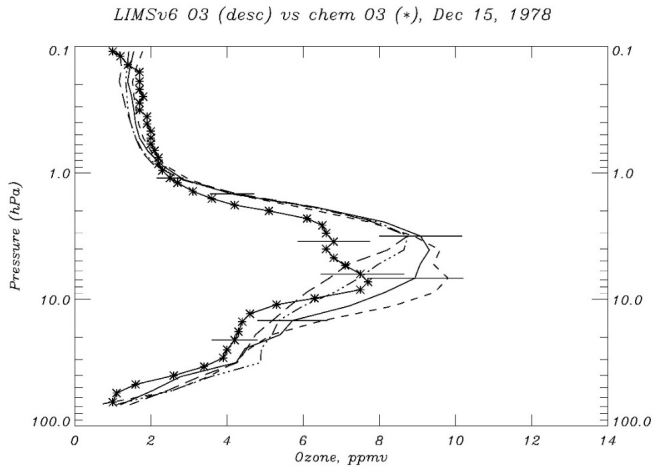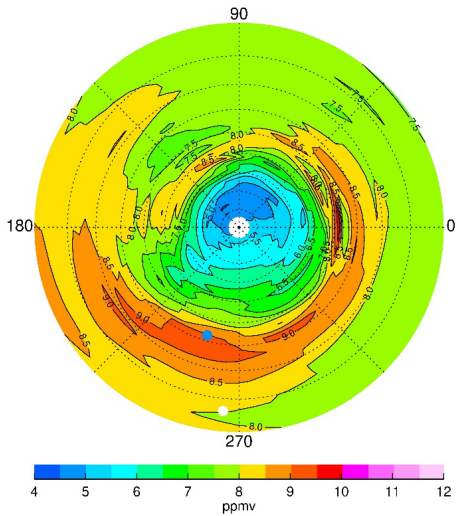
Figure 4—(top) Profiles of V6 ozone (at 0611Z) versus rocket chem ozone (* at 0541Z) on

December 15. The four V6 profiles have separations of 2.6° latitude, and the solid curve (at

31.8°N) is closest to White Sands (WS, 32.4°N). Horizontal bars are ozone errors. (bottom) NH

V6 ozone at 4.6 hPa; Greenwich (0°E) is at right, and CI is 0.5 ppmv. Latitude (dotted circles) is

every 10°. Satellite location is white dot (6°N, 265°E), and WS is blue dot.

557

558

559
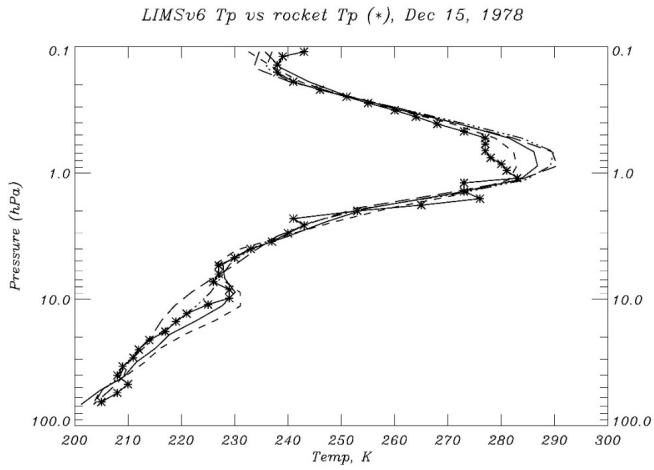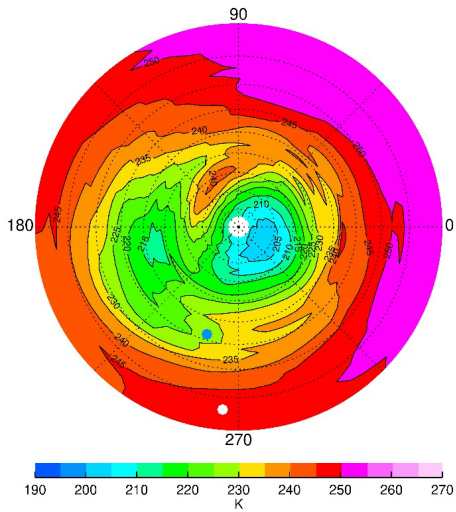
Figure 5—(top) Profiles of V6 temperature compared with Datasonde values (*) on December 15. The four V6 profiles are separated as in Fig. 4, where the short-dashed curve is for 29.2° and the long-dashed curve is for 37.2°. (bottom) NH V6 temperature distribution at 4.6 hPa; CI is 5 K, and satellite location is white dot and White Sands is blue dot.

564

565

566

567
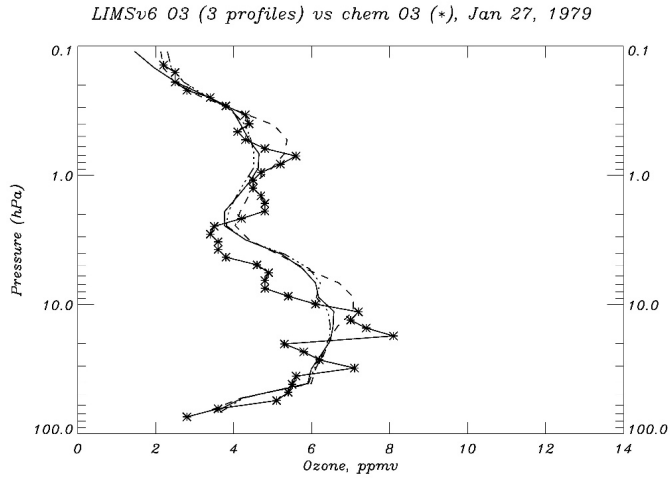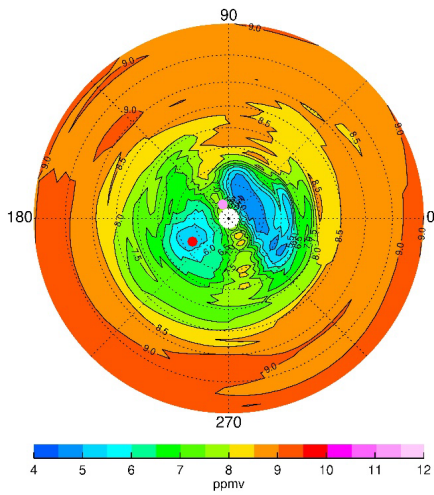
Figure 6—(top) As in Fig. 4, but for January 27, 1979, at Poker Flat, AK (65°N, 212.5°E);

(bottom) NH V6 distribution of ozone at 4.6 hPa, where CI is 0.5 ppmv. Latitudes (dotted

circles) are spaced every 10°; Poker Flat is red and satellite position (81°N, 113°E) is pink.

571

572

573

574

575

576
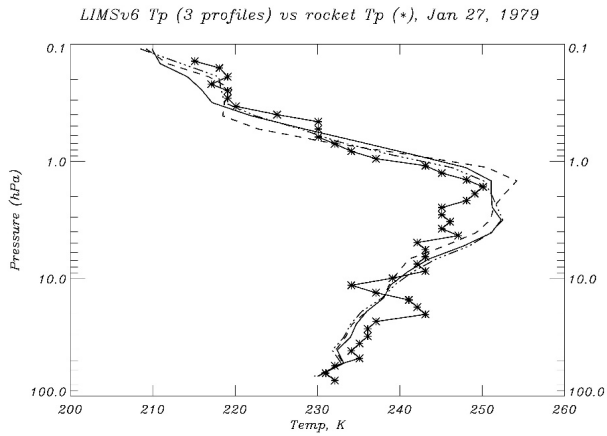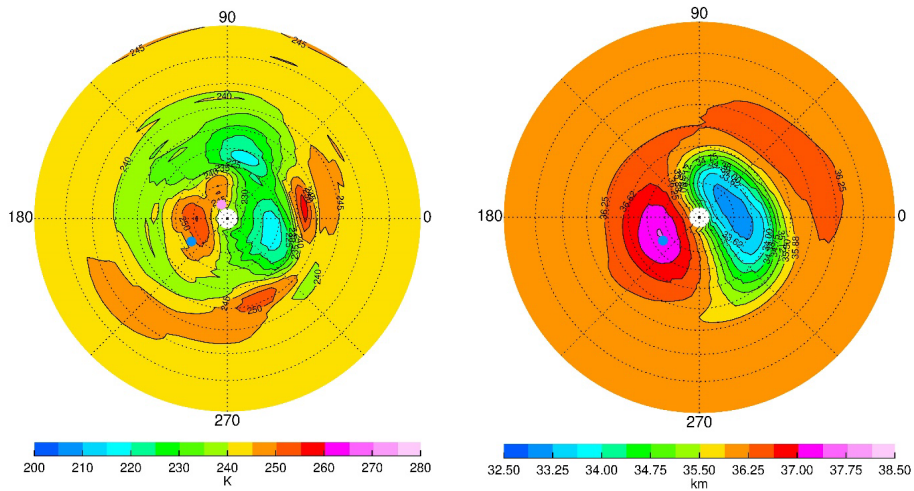
Figure 7—(top) As in Fig. 5, but for January 27, 1979. (bottom-left) NH V6 temperature; CI is 5

K. Poker Flat is blue and satellite position is pink. (bottom-right) V6 GPH; CI is 0.375 gpkm.

579

580
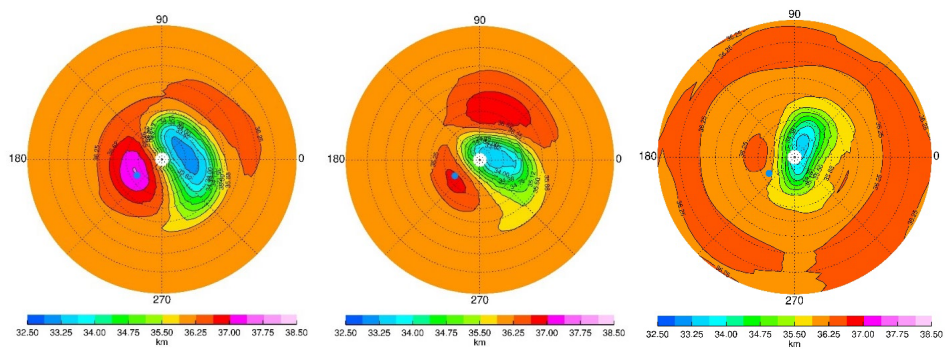
Figure 8—NH V6 GPH at 4.6 hPa; CI is 0.375 gpkm. Poker Flat is blue dot. Panels are spaced

one week apart; (left) February 3; (middle) February 10; and (right) February 17.

583
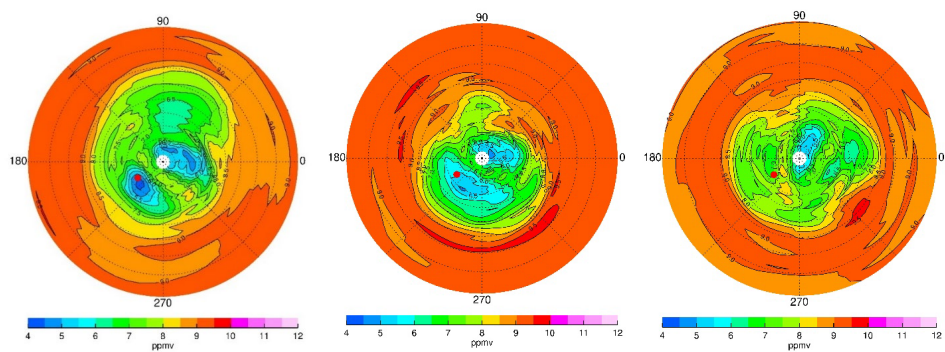
584

585

586 Figure 9—Maps of ozone at 4.6 hPa (left) on February 3, (middle) on February 10; and (right) on

587 February 17. CI is 0.5 ppmv and red dot is Poker Flat.

588
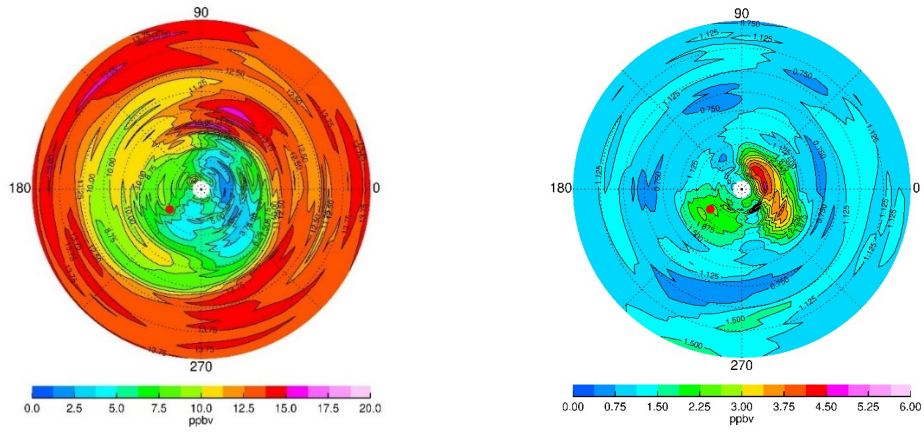
599

600

601 Figure 10—(left) Nighttime NO_2 on January 27 at 4.6 hPa; CI is 1.25 ppbv. (right) HNO_3 at 4.6

602 hPa; CI is 0.375 ppbv. Red dot is Poker Flat.

603

604

605

Jan 28,1979, 09Z, 5 hPa, 212E, 64N
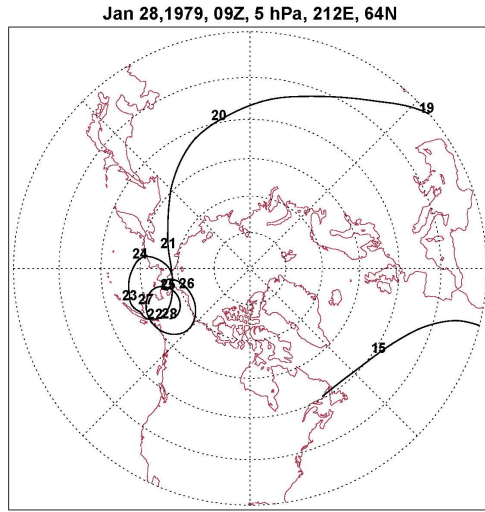
606

607 Figure 11—Trajectory of air parcel that end on January 28 at the location of the LOP. Numbers
608 on the trajectory denote the date, beginning with January 15 and where the parcel is equatorward
609 of 30°N on January 16-18.

610
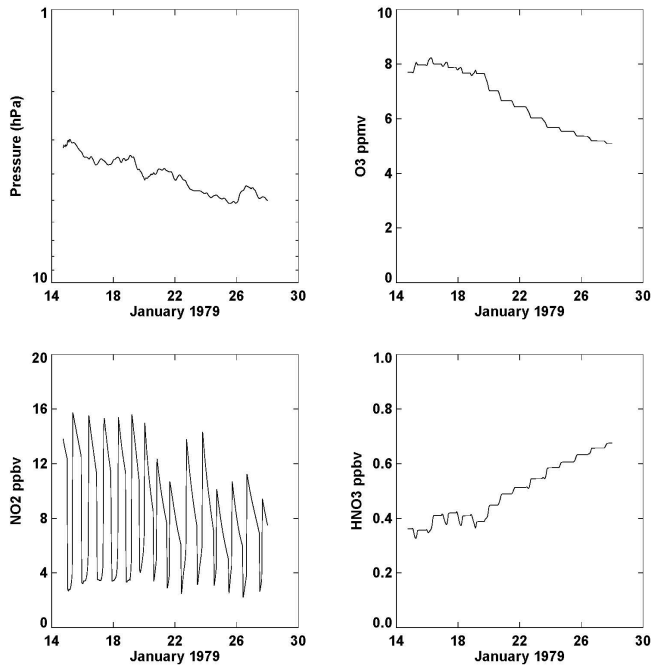
Figure 12—Air parcel history of the changes in its (top left) pressure, (top right) ozone, (bottom left) NO$_2$, and (bottom right) HNO$_3$.

624
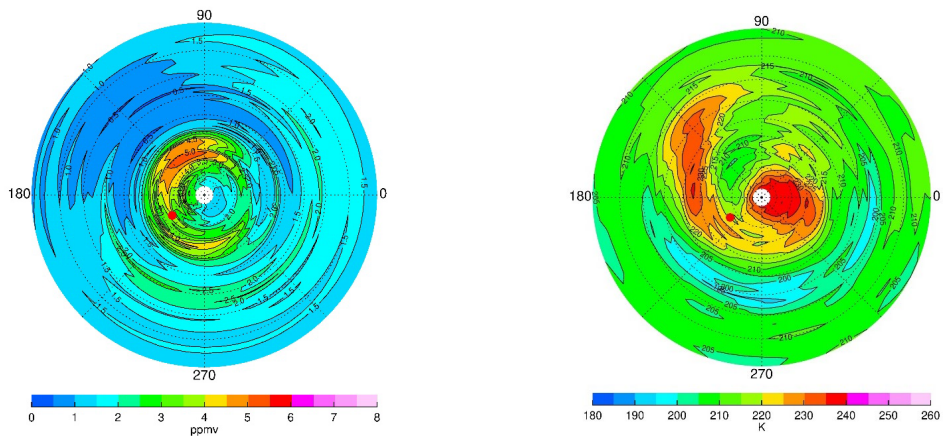
625 Figure ~~11~~13—(top) NH distributions for December 15 at 0.022 hPa for (left) ozone and for

626 (right) temperature; CIs are 0.5 ppmv and 5 K, respectively. Red dot denotes location of Poker

627 Flat.

628

629

630

631

632
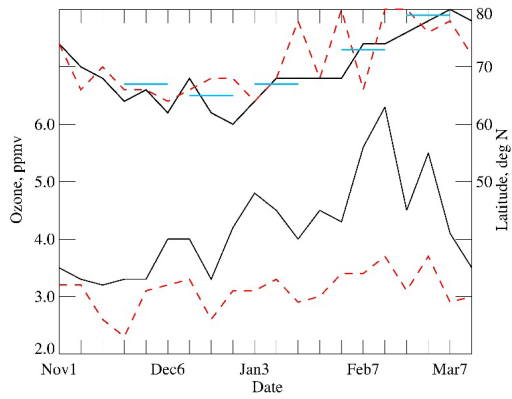
633

634   Figure ~~12~~14—Time series of peak V6 ozone (bottom two curves) and its latitude location (top

635   two curves) at 0.022 hPa. Dashed red curves are for combined ozone, while solid curves are for

636   descending (nighttime) ozone only. Horizontal blue lines indicate the latitude of the terminator.

637

638
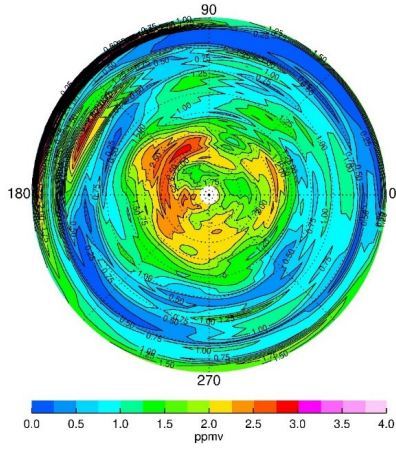
639

640

641   Figure ~~13~~15—NH V6 combined (A+D) ozone distribution at 68 hPa for December 15, 1978. CI

642   is 0.25 ppmv.

643

References

Andrews, D. G., Holton, J. R., and Leovy, C. B.: *Middle Atmosphere Dynamics*, 1st Ed., 489 pp., Academic Press, 1987.

Chandran, A., Collins, R. L., Garcia, R. R., Marsh, D. L., Harvey, V. L., Yue, J., and de la Torre, L.: A climatology of elevated stratopause events in the whole atmosphere community climate model, J. Geophys. Res. Atmos., 118, 1234-1246, https://doi.org/10.1002/jgrd.50123, 2013.

de la Cámara, A., Abalos, M., Hitchcock, P., Calvo, N., and Garcia, R. R.: Response of Arctic ozone to sudden stratospheric warmings, Atmos. Chem. Phys., 18, 16499–16513, https://doi.org/10.5194/acp-18-16499-2018, 2018.

Edwards, D. P., Kumer, J. B., Lopez-Puertas, M., Mlynczak, M. G., Gopalan, A., Gille, J. C., and Roche, A.: Non-local thermodynamic equilibrium limb radiance near 10 μm as measured by UARS CLAES, J. Geophys. Res., 101, D21, 26,577-26,588, https://doi.org/10.1029/96JD02133, 1996.

Fleming, E.L., Chandra, S., Barnett, J. J., and Corney, M.: Zonal mean temperature, pressure, zonal wind, and geopotential height as functions of latitude, COSPAR International Reference Atmosphere: 1986, Part II: Middle Atmosphere Models, Adv. Space Res., 10 (12), 11-59, https://doi.org/10.1016/0273-1177(90)90386-E, 1990.

Funke, B., López-Puertas, M., Garcia-Comas, M., Kaufmann, M., Höpfner, M., and Stiller, G. P.: GRANADA: a generic RAdiative traNsfer AnD non-LTE population algorithm, J. Quant. Spectros. Radiat. Transfer, 113, 1771–1817, https://doi.org/doi: 10.1016/j.jqsrt.2012.05.001, 2012.

671   Gettelman, A., Hoor, P., Pan, L. L., Randel, W. J., Hegglin, M. I., and Birner, T.: The

672   extratropical upper troposphere and lower stratosphere, Rev. Geophys., 49, RG3033,

673   https://doi.org/10.1029/2011RG000355, 2011.

674

675   Gille, J. C. and Russell III, J. M.: The limb infrared monitor of the stratosphere: experiment

676   description, performance, and results, J. Geophys. Res., 84, 5125-5140,

677   https://doi.org/10.1029/JD089iD04p05125, 1984.

678

679   Harvey, V. L., Pierce, R. B., Hitchman, M. H., Randall, C. E., and Fairlie, T. D.: On the

680   distribution of ozone in stratospheric anticyclones, J. Geophys. Res., 109, D24308,

681   https://doi:10.1029/2004JD004992, 2004.

682

683   Harvey, V. L., Randall, C. E., Manney, G. L., and Singleton, C. S.: Low-ozone pockets observed

684   by EOS-MLS, J. Geophys. Res., 113, D17112, https://doi.org/10.1029/2007JD009181, 2008.

685

686   Hegglin, M. I., Tegtmeier, S., Anderson, J., Bourassa, A. E., Brohede, S., Degenstein, D.,

687   Froidevaux, L., Funke, B., Gille, J., Kasai, Y., Kyrola, E. T., Lumpe, J., Murtagh, D., Neu, J. L.,

688   Perot, K., Remsberg, E. E., Rozanov, A., Toohey, M., Urban, J., von Clarmann, T., Walker, K.

689   A., Wang, H-J.., Arosio, C., Damadeo, R., Fuller, R. A., Lingenfelser, G., McLinden, C.,

690   Pendelbury, D., Roth, C., Ryan, N. J., Sioris, C., Smith, L., and Weigel, K.: Overview and update

691   of the SPARC Data Initiative: comparison of stratospheric composition measurements from

692   satellite limb sounders, Earth Syst. Sci. Data, 13, 1855-1903, https://doi.org/10.5194/essd-1855-

693   2021, 2021.

694

695   Hilsenrath, E.: Rocket observations of the vertical distribution of ozone in the polar night and

696   during a mid-winter stratospheric warming, Geophys. Res. Lett., 7, 581-584,

697   https://doi.org/10.1029/GL007i008p00581, 1980.

698

Hilsenrath, E., and Kirschner, P. T.: Recent assessment of the performance and accuracy of a
chemiluminescent rocket sonde for upper atmospheric ozone measurements, Rev. Sci. Instrum.,
Vol. 51, 1381-1389, https://doi.org/10.1063/1.1136080, 1980.

702

Hitchman, M. H., Gille, J. C., Rodgers, C. D., and Brasseur, G.: The separated polar winter
stratopause: a wave driven climatological feature, J. Atmos. Sci., 46, 410-422,
https://doi.org/10.1175/1520-0469(1989)046%3C0410:TSPWSA%3E2.0.CO;2, 1989.

706

Holt, L. A., Randall, C. E., Harvey, V. L., Remsberg, E. E., Stiller, G. P., Funke, B., Bernath, P.
F., and Walker, K. A., Atmospheric effects of energetic particle precipitation in the Arctic winter
1978–1979 revisited, J. Geophys. Res., 117, D05315, https://doi.org/10.1029/2011JD016663,
2012.

711

Kim, J-H., Jee, G., Choi, H., Kim, B-M., and Kim, S-J.: Vertical structures of temperature and
ozone changes in the stratosphere and mesosphere during stratospheric sudden warmings, J.
Astron. Space Sci., 37, 69-75, https://doi.org/10.5140/JASS.2020.37.1.69, 2020.

715

Leovy, C. B., Sun, C-R., Hitchman, M. H., Remsberg, E. E., Russell, III, J. M., Gordley, L. L.,
Gille, J. C., and Lyjak, L. V.: Transport of ozone in the middle stratosphere: evidence for
planetary wave breaking, J. Atmos. Sci., 42, 230-244, https://doi.org/10.1175/1520-
0469(1985)042%3C0230:TOOITM%3E2.0.CO;2, 1985.

720

Lieberman, R. S., Oberheide, J., Hagan, M. E., Remsberg, E. E., and Gordley, L. L.: Variability
of diurnal tides and planetary waves during November 1978–May 1979, J. Atmos. Solar-Terr.
Phys., 66, 517–528, https://doi.org/10.1016/j.jastp.2004.01.006, 2004.

724

Lopez-Puertas, M. and Taylor, F. W.: Non-LTE Radiative transfer in the Atmosphere, World
Scientific Publ. Co., River Edge, NJ, USA, 504 pp., 2001.

López-Puertas, M., García-Comas, M., Funke, B., Gardini, A., Stiller, G. P., Clarmann, T. von,
Glatthor, N., Laeng, A., Kaufmann, M., Sofieva, V. F., Froidevaux, L., Walker, K. A., and
Shiotani, M.: MIPAS observations of ozone in the middle atmosphere, Atmos. Meas. Tech., 11,
2187–2212, https://doi.org/10.5194/amt-11-2187-2018, 2018.

Manney, G. L., Froidevaux, L., Waters, J. W., Zurek, R. W., Gille, J. C., Kumer, J. B.,
Mergenthaler, J. L., Roche, A. E., O'Neill, A., and Swinbank, R.: Formation of low-ozone
pockets in the middle stratospheric anticyclone during winter, J. Geophys. Res. Atmos., 100,
13939-13950, https://doi.org/10.1029/95JD00372, 1995.

Marsh, D., Smith, A., Brasseur, G., Kaufmann, M., and Grossmann, K.: The existence of a
tertiary ozone maximum in the high-latitude middle mesosphere, Geophys. Res. Lett., 28, 4531-
4534, https://doi.org/10.1029/2001GL013791, 2001.

Manuilova, R. O., Gusev, O. A., Kutepov, A. A., von Clarmann, T., Oelhaf, H., Stiller, G. P,
Wegner, A., Lopez-Puertas, M., Martin-Torres, F. J., Zaragoza, G., and Flaud, J.-M.: Modelling
of non-LTE limb spectra of i.r. ozone bands for the MIPAS space experiment, J. Quant.
Spectrosc. Rad. Transf., 59, 405-422, https://doi.org/10.1016/S0022-4073(97)00120-9, 1998.

Mlynczak, M. G. and Drayson, R.: Calculation of infrared limb emission by ozone in the
terrestrial middle atmosphere 2. Emission calculations, J. Geophys. Res., 95, 16,513-16,521,
https://doi.org/10.1029/JD095iD10p16513, 1990.

751 Morris, G. A., Kawa, S. R., Douglass, A. R., Schoeberl, M. R., Froidevaux, L., and Waters, J.,
752 Low-ozone pockets explained, J. Geophys. Res., 103, 3599-3610,
753 https://doi.org/10.1029/97JD02513, 1998.

754

755 Nair, H., Allen, M., Froidevaux, L., and Zurek, R.: Localized rapid ozone loss in the northern
756 winter stratosphere: An analysis of UARS observations, J. Geophys. Res., 103, 1555-1571,
757 https://doi.org/10.1029/97JD03072, 1998.

758

759 Remsberg, E., and Lingenfelser, G.: LIMS Version 6 Level 3 dataset, NASA-TM-2010-216690,
760 available at http://www.sti.nasa.gov (last access: 17 September 2019), 13 pp., 2010.

761

762 Remsberg, E. E., Haggard, K. V., and Russell III, J. M.: Estimation of synoptic fields of middle
763 atmosphere parameters from Nimbus-7 LIMS profile data, J. Atmos. Ocean. Tech, 7, 689-705,
764 https://doi.org/10.1175/1520-0426(1990)007%3C0689:EOSFOM%3E2.0.CO;2, 1990.

765

766 Remsberg, E. E., Gordley, L. L, Marshall, B. T., Thompson, R. E., Burton, J., Bhatt, P., Harvey,
767 V. L., Lingenfelser, G., Natarajan, M.: The Nimbus 7 LIMS version 6 radiance conditioning and
768 temperature retrieval methods and results, J. Quant. Spectros. Rad. Transf., 86, 395-424,
769 doi:10.1016/j.jqsrt.2003.12.007, 2004.

770

771 Remsberg, E., Lingenfelser, G., Natarajan, M., Gordley, L., Marshall, B. T., and Thompson, E.:
772 On the quality of the Nimbus 7 LIMS version 6 ozone for studies of the middle atmosphere, J.
773 Quant. Spectros. Rad. Transf., 105, 492-518, doi:10.1016/j.jqsrt.2006.12.005, 2007.

774

775 Remsberg, E., Lingenfelser, G., and Natarajan, M.: LIMS/Nimbus-7 Level 3 Daily 2 deg
776 Latitude Zonal Fourier Coefficients of O3, NO2, H2O, HNO3, Geopotential Height, and
777 Temperature V006, Version: 006, Goddard Earth Sciences Data and Information Services Center

(GES DISC), available at: https://disc.gsfc.nasa.gov/datacollection/LIMSN7L3_006.html (last
access: 11 March 2021), 2011.

Remsberg, E., Natarajan, M., Fairlie, T. D., Wargan, K., Pawson, S., Coy, L., Lingenfelser, G.,
and Kim, G.: On the inclusion of Limb Infrared Monitor of the Stratosphere version 6 ozone in a
data assimilation system, J. Geophys. Res., 118, 7982-8000, https://doi.org/10.1002/jgrd.50566,
2013.

Remsberg. E., Natarajan, M., and Harvey, V. L.: On the consistency of HNO_3 and NO_2 in the
Aleutian High region from the Nimbus 7 LIMS Version 6 dataset, Atmos. Meas. Tech., 11,
3611-3626, https://doi.org/10.5194/amt-11-3611-2018, 2018.

Remsberg, E., Harvey, V. L., Krueger, A., and Natarajan, M.: Residual temperature bias effects
in stratospheric species distributions from LIMS, Atmos. Meas. Tech., 14, 2185-2199,
https://doi.org/10.5194/amt-14-2185-2021, 2021.

Shams, S. B., von Walden, P., Hannigan, J. W., Randel, W. J., Petropavlovskikh, I. V., Butler, A.
H., and de la Cámara, A.: Analyzing ozone variations and uncertainties at high latitudes during
sudden stratospheric warming events using MERRA-2, Atmos. Chem. Phys. Disc.,
https://doi.org/10.5194/acp-2021-646, 2021.

Shepherd, T. G., Plummer, D. A., Scinocca, J. F., Hegglin, M. I., Fioletov, V. E., Reader, M. C.,
Remsberg, E., von Clarmann, T., and Wang, H. J.: Reconciliation of halogen-induced ozone loss
with the total-column record, Nature Geoscience, 7, 443-449, doi:10.1038/ngeo2155, 2014.

803   Siskind, D. E., Coy, L., Espy, P.: Observations of stratospheric warmings and mesospheric

804   coolings by the TIMED SABER instrument, Geophys. Res. Lett. 32,

805   http://doi.org/10.1029/2005GL022399, 2005.

806

807   Siskind, D. E., Harvey, V. L., Sassi, F., McCormack, J. P., Randall, C. E., Hervig, M. E., and

808   Bailey, S. M.: Two- and three-dimensional structures of the descent of mesospheric trace

809   constituents after the 2013 sudden stratospheric warming elevated stratopause event, Atmos.

810   Chem. Phys., 21, 14059–14077, https://doi.org/10.5194/acp-21-14059-2021, 2021.

811

812   Smith, A. K., López-Puertas, M., García-Comas, M., and Tukiainen, S.: SABER observations of

813   mesospheric ozone during NH late winter 2002–2009, Geophys. Res. Lett., 36, L23804,

814   https://doi.org/10.1029/2009GL040942, 2009.

815

816   Smith, A. K., Garcia, R. R., Marsh, D. R., and Richter, J. A.: WACCM simulations of the mean

817   circulation and trace species transport in the winter mesosphere, J. Geophys. Res., 116, D20115,

818   **https://doi.org/10.1029/2011JD016083,** 2011.

819

820   Smith, A. K., Espy, P. J., López-Puertas, M., and Tweedy, O. V., Spatial and temporal structure

821   of the tertiary ozone maximum in the polar winter mesosphere, J. Geophys. Res., 123, 4373-

822   4389, https://doi.org/10.1029/2017JD028030, 2018.

823

824   Sofieva, V. F., Szelą M., Tamminen, J., Kyrölä, E., Degenstein, D., Roth, C., Zawada, D.,

825   Rozanov, A., Arosio, C., Burrows, J. P., Weber, M., Laeng, A., Stiller, G. P., von Clarmann, T.,

826   Froidevaux, L., Livesey, N., van Roozendael, M., and Retscher, C.: Measurement report:

827   regional trends of stratospheric ozone evaluated using the MErged GRIdded Dataset of Ozone

828   Profiles (MEGRIDOP), Atmos. Chem. Phys., 21, 6707–6720, https://doi.org/10.5194/acp-21-

829   6707-2021, 2021.

830

Solomon, S., Kiehl, J. T., Kerridge, B. J., Remsberg, E. E., and Russell III, J. M.: Evidence for nonlocal thermodynamic equilibrium in the ν_3 mode of mesospheric ozone, J. Geophys. Res., 91, 9865-9876, https://doi.org/10.1029/JD091iD09p09865, 1986.

834

SPARC, Assessment of Stratospheric Aerosol Properties, L. Thomason and Th. Peter, Ed., WCRP-124, WMO/TD- No. 1295, SPARC Report No. 4, 322 pp., 2006.

837

SPARC: The SPARC Data Initiative: Assessment of stratospheric trace gas and aerosol climatologies from satellite limb sounders, Hegglin, M. I. and Tegtmeier, S., (Eds.), SPARC Report No. 8, WCRP-5/2017, http://www.sparc-climate.org/publications/sparc-reports/, 2017.

841

Stolarski, R. S., Douglass, A. R., Remsberg, E. E., Livesey, N. J., and Gille, J. C.: Ozone temperature correlations in the upper stratosphere as a measure of chlorine content, J. Geophys. Res., 117, D10305, https://doi.org/10.1029/2012JD017456. 2012.

845

Tegtmeier, S., Hegglin, M. I., Anderson, J., Bourassa, A., Brohede, S., Degenstein, D., Froidevaux, L., Fuller, R., Funke, B., Gille, J., Jones, A., Kasai, Y., Krüger, K., Kyrölä, E., Lingenfelser, G., Lumpe, J., Nardi, B., Neu, J., Pendlebury, D., Remsberg, E., Rozanov, A., Smith, L., Toohey, M., Urban, J., von Clarmann, T., Walker, K. A. and Wang, R. H. H.: SPARC Data Initiative: A comparison of ozone climatologies from international satellite limb sounders, J. Geophys. Res., 118, 12,229-12,247, https://doi.org/10.1002/2013JD019877, 2013.

852

WOUDC, World Ozone and Ultraviolet Radiation Data Centre, https://woudc.org/home.php.

854

855